Label-free monitoring of drug-induced cytotoxicity and its molecular fingerprint by live-cell Raman and autofluorescence imaging

Menglu Li[1,2]*, Hao-Xiang Liao[1], Kazuki Bando[1], Yasunori Nawa[1,2], Satoshi Fujita[1,2], Katsumasa Fujita[1,2,3]*

AFFILIATIONS:

[1]Department of Applied Physics, Osaka University, 2-1 Yamadaoka, Suita, Osaka 565-0871, Japan.

[2]AIST-Osaka University Advanced Photonics and Biosensing Open Innovation Laboratory, National Institute of Advanced Industrial Science and Technology (AIST), Suita, Osaka 565-0871, Japan.

[3]Institute for Open and Transdisciplinary Research Initiatives, Osaka University, 2-1 Yamadaoka, Suita, Osaka 565-0871, Japan.

*Correspondence to: Menglu Li, Katsumasa Fujita

EMAIL: menglu.li@ap.eng.osaka-u.ac.jp, fujita@ap.eng.osaka-u.ac.jp

ABSTRACT

Simultaneous observation of drug distribution at the effector site and subsequent cell response is essential in the drug development process. However, few studies have visualized the drug itself and biomolecular interactions in living cells. Here, we used label-free Raman microscopy to investigate drug-induced cytotoxicity and visualize drug uptake and subcellular localization by its specific molecular fingerprint. The redox-sensitive Raman microscope detected the decrease of reduced cytochrome *c* (cyt *c*) after Actinomycin D (ActD) treatment at a time-dependent and dose-dependent format. Immunofluorescence staining of cyt *c* suggested that the release of cyt *c* was not the major cause. Combining Raman microscopy with conventional biological methods, we reported that the oxidization of cyt *c* is an early cytotoxicity marker prior to the release of cyt *c*. Moreover, as the spectral properties of ActD are sensitive to the surrounding environment, subcellular localization of ActD was visualized sensitively by the weak autofluorescence, and the intercalation of ActD into DNA was detected by shifted Raman peak, allowing for parallel observation of drug uptake and the mechanism of action. In this research, we achieved simultaneous observation of cytotoxicity and cellular drug uptake by Raman microscopy, which could facilitate a precise understanding of pharmacological effects and predict potential drug toxicity in the future.

INTRODUCTION

Since the first chemotherapy successfully blocked tumor progression in 1942, chemotherapy has remained one of the leading strategies for cancer treatment, driving the anticancer drug industry.[1] Cancer cells go rogue by escaping from the control of cell division and evading programmed cell death.[2] Therefore, a main target of chemotherapeutic drugs is to induce cell apoptosis targeting DNA replication or protein synthesis.[3] Screening chemotherapeutic drugs for cancer treatment requires the investigation of cytotoxicity and drug uptake to understand the drug mechanism of action. However, the lack of efficient methods to visualize intracellular drug distribution hinders detailed investigation of the drug effect at the target site.[4] A technique that can visualize drug uptake and subsequent cellular response on-site in living and single-cell formats will facilitate a precise understanding of the pharmacological effect of chemotherapeutic drugs.

Raman microscopy has emerged as a powerful analytical tool for investigating drug-cell interactions since it can detect molecular fingerprints given by the intrinsic chemical structures of both cells and drugs without additional sample preparation.[5-7] A drug with distinct spectroscopic features compared with the cellular Raman spectra can be detected and visualized. One common strategy is to utilize bioorthogonal Raman labels which the characteristic peaks arise at the cell-silent region, such as alkyne and deuterium.[8,9] Stimulated Raman scattering (SRS) microscopy has been applied to image alkyne or deuterium-labeled small molecules with high sensitivity and fast acquisition.[10, 11] However, optical window for intrinsic cellular signatures is limited. Spontaneous Raman microscopy covers fingerprint, cell-silent, and C-H vibration regions, providing a wider optical window for biochemical information. Naturally alkyne-containing drugs, such as erlotinib and neratinib, and the metabolites were investigated together will cellular information.[12, 13] In addition to the Raman peaks in the cell-silent region, distinguishable Raman peaks in the fingerprint region were

applied to understand the subcellular distribution of doxorubicin, paclitaxel, and theraphthal and the subsequent cellular responses.[14-16] Combined with autofluorescence imaging, the localization of anthraycine in nuclei was visualized and cellular response was studied by Raman microscopy.[17] However, most studies measured fixed or air-dried cell samples, which missing real-time information. Also, Raman scattering is sensitive to conformation changes in drug molecules, such as the change caused by intercalation into DNA, which allows us to investigate this feature in living cell conditions.

Actinomycin D (ActD), the first antibiotic shown to have anticancer activity, was isolated in 1940 and approved for medical use in 1964.[18] Act D preferentially intercalates into GC-rich sequences and inhibits DNA transcription[19, 20], which generally leads to cell apoptosis. The interaction between ActD and DNA have been evaluated by adsorption, fluorescence, and Raman spectroscopy. The absorption spectrum of ActD shifted to the longer wavelengths when complexed with DNA, while the excitation spectrum of ActD shifted to the shorter wavelength.[21, 22] The ratio between the intensity of Raman shifts at 1505 cm^{-1} and 1489 cm^{-1} was used to estimate binding affinity of ActD to DNA.[23] However, this difference is more likely due to different solvents but not binding to DNA. Smulevich *et al.* reported the Raman profiles of ActD-DNA complex in water excited at several different wavelengths.[24] The Raman intensity of characteristic peaks, including 1487 cm^{-1}, 1404 cm^{-1}, 1263 cm^{-1}, and 1213 cm^{-1} increased while no obvious shifts of bands were mentioned. An *in vitro* study of the interaction of Act D with cancer cells using Raman micro-spectroscopy was reported by Farhane *et al.*[25] A decrease in the Raman signatures of nucleic acids was reported which is related to the mechanism of action. However, no specific Raman shifts of the ActD spectrum were detected in the cellular spectra. As far as we know, no paper reported successful observation of ActD or its DNA complex in living cells by Raman microscopy. Therefore, we chose ActD as a model

drug to investigate its molecular fingerprint including Raman signature and autofluorescence in living cells by Raman microscopy.

We have developed a line-illumination Raman microscope that allows for acquiring several hundred spectra with one exposure, thus enabling the visualization of living cells at a spatial resolution comparable to that of laser scanning confocal microscopy.[26] We previously visualized the dynamics of cytochrome *c* (cyt *c*) during cell apoptosis and cell division using our homemade line-illumination Raman microscope.[27, 28] In the present study, we further monitored drug-induced cytotoxicity and changes in molecular fingerprint at a real-time and single-cell format by Raman microscopy. In this study, we cultured HeLa cells with ActD and simultaneously monitored ActD uptake and the subsequent cellular response. The characteristic Raman shifts after ActD binding with nucleic acids were detected, which directly proved that ActD intercalates into double-stranded DNA. We demonstrated that Raman-based measurement of drug-induced cytotoxicity is more sensitive, rapid, and information-rich than the conventional 3-(4,5-dimethyl-2-thiazolyl)-2,5-diphenyl-2H-tetrazolium bromide (MTT) assay and can be an alternative method to screen drug-induced cytotoxicity and approach to the mechanism of action in the future.

RESULTS AND DISCUSSION

Simultaneous observation of drug uptake and cellular response

HeLa cells were treated with 0.1 μM ActD for 4 h, and hyperspectral Raman images were captured. A typical Raman spectrum of HeLa cells under 532 nm excitation is dominated by the major vibration modes of reduced cytochromes at 600, 750, 1130, 1314, and 1585 cm^{-1}.[27] In addition to the typical Raman signatures of HeLa cells, we detected a fluorescence signal from ActD inside the cells. The spectra showed a blueshift compared to the fluorescence

spectrum of ActD in aqueous solution (Figure S1). Chinsky *et al.* reported an alteration of the fluorescence spectrum of ActD in different solvents, and a blueshift of the emission maximum occurred once ActD bound to DNA,[22] which suggested that the blueshift and the enhancement of fluorescence observed in our study may be due to the binding of ActD to DNA. Therefore, we used the autofluorescence region (1950 cm^{-1} to 2250 cm^{-1}) to visualize the distribution of ActD (Figure 1A, magenta). Cellular heterogeneity in ActD uptake was found using autofluorescence imaging.

Subsequently, a significant decline in Raman shifts at 600, 750, 1130, 1314, and 1585 cm^{-1}), that can be assigned to reduced cytochromes, was observed in cells whose nuclei were fulfilled with the autofluorescence signal (Figure 1B). The excitation at 532 nm enhances cytochrome *b* (cyt *b*) and *c* (cyt *c*), containing heme *b* and *c* as a co-factor, respectively. The Raman shift at 600 cm^{-1} can be used to distinguish reduced cyt *c* from cyt *b*.[29] The tendency of 750, 1130, 1314, and 1585 cm^{-1} correlated with that of 600 cm^{-1} (Figure S2), indicating the major contribution of cyt *c* in the response to ActD treatment. Therefore, the Raman peaks at 750, 1130, 1314, and 1585 cm^{-1} were considered to represent the distribution of reduced cyt *c* in this measurement.

Figure 1A shows the distribution of the Raman signal at 1585 cm^{-1} and 1950-2250 cm^{-1} to investigate the relation between the drug uptake and subsequent cellular response. Except the decline in the signal of 1585 cm^{-1} in cells with drug uptake, we also found that the signal of 1585 cm^{-1} did not change in cells that had not initiated uptake or were in the process of uptake. The right “half-moon” contrast of ActD observed in the nuclei, which is indicated by the white arrow, showed that drug uptake proceeded while the illumination line scanned the cells. Figure 1 also shows the heterogeneity of cellular drug uptake and cellular response, which is important to understand drug effects comprehensively. The heterogeneity of the cellular

response to drug treatment might cause the failure of anticancer drugs. This result suggested that the difference in cellular response may originate from the different speeds of drug uptake.

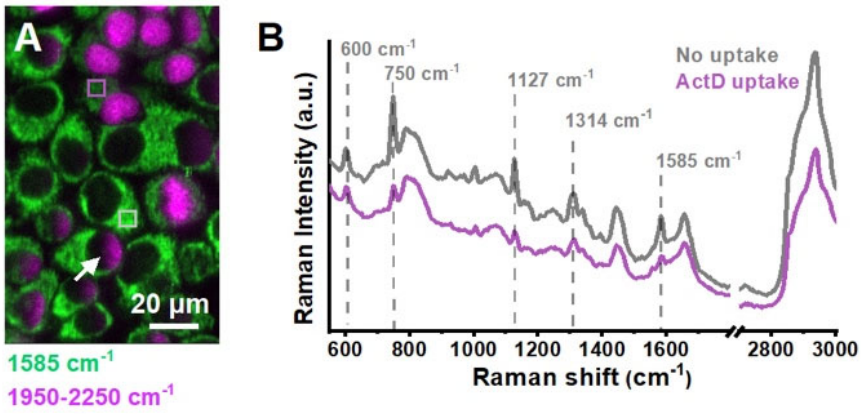

Figure 1. Raman spectral images of HeLa cells treated with ActD. (A) The Raman images at 1585 cm^{-1} and 1950-2250 cm^{-1} were reconstructed. Scale bar, 20 μm. (B) Comparison of the average spectra obtained from cytosol of the cells where ActD uptake has begun (purple trace) and not yet started (gray trace). The areas used for averaging spectra were framed by purple and gray squares (20 pixels × 20 pixels) in Figure 1A. Power density of incident laser is 3 $mW/\mu m^2$.

Detection of drug-induced cytotoxicity earlier than the MTT assay by Raman microscopy

Next, we investigated the time-dependent manner of cellular drug uptake and the effect on cyt *c* dynamics. HeLa cells were treated with 1 μM ActD and incubated for 0.5, 1, 2, 4, and 8 h. Cells without ActD treatment were used as controls. Raman observation was performed at each time point, followed by the MTT assay as a comparison. To avoid possible photodamage from laser light, we chose a laser power of 1 mW/μm^2 for the following experiments after performing photodamage test as shown in Figure S3 and S4. A live/dead assay following Raman measurement was also performed to measure cell viability after Raman measurement. We did not find a viability change detectable in Raman imaging area (Figure S5). We observed a decline in cyt *c* intensity with the accumulation of ActD, as shown in Figure 2A. At 0.5 h, we observed that the drug signal occupied the right half of the nuclei, which may indicate drug uptake during the measurement. In Figure 2A, the line was scanned from left to right while imaging (see Methods). This "half-moon" effect was not detected after 2 h when drug uptake was saturated, indicating that drug uptake was completed for all cells in the field of view in 2 hours. The same phenomenon appeared when cells were treated with a low concentration of ActD for a longer incubation time, as shown in Figure 1A.

Cell viability at different time points was measured by the conventional MTT assay, which is based on the conversion of water-soluble tetrazolium salt into water-insoluble purple formazan crystals by cellular oxidoreductase in living cells.[30] Following the quantification of dissolved formazan using colorimetric analysis, the number of metabolically active cells was estimated. The MTT assay indicated a significant cytotoxic effect after treatment with 1 μM ActD for 4 h (Figure 2B), while the Raman-based method showed a faster decline in the cyt *c* signal at 0.5 h (Figure 2A) when cells started to take up ActD. This result suggested that Raman microscopy can detect drug-induced cytotoxicity earlier than the conventional MTT assay.

Morimoto *et al.* also reported that Raman microscopy can detect mitochondrial dysfunction in neuronal cells earlier than MTT assays, which is consistent with our result.[31]

Although the MTT assay is a widely used cell viability assay, a major disadvantage is that injured mitochondria may still be able to reduce MTT to formazan crystals, leading to a false-positive result of cell viability and relatively low sensitivity.[32] Other concerns include the possible changes in reductase activity due to the test substances or the cytotoxicity of the MTT substrate, which may lead to an overestimation or underestimation of cell viability.[33] Because Raman-based measurements did not use external reagents or complex processing, cell viability could be monitored under natural physiological conditions.

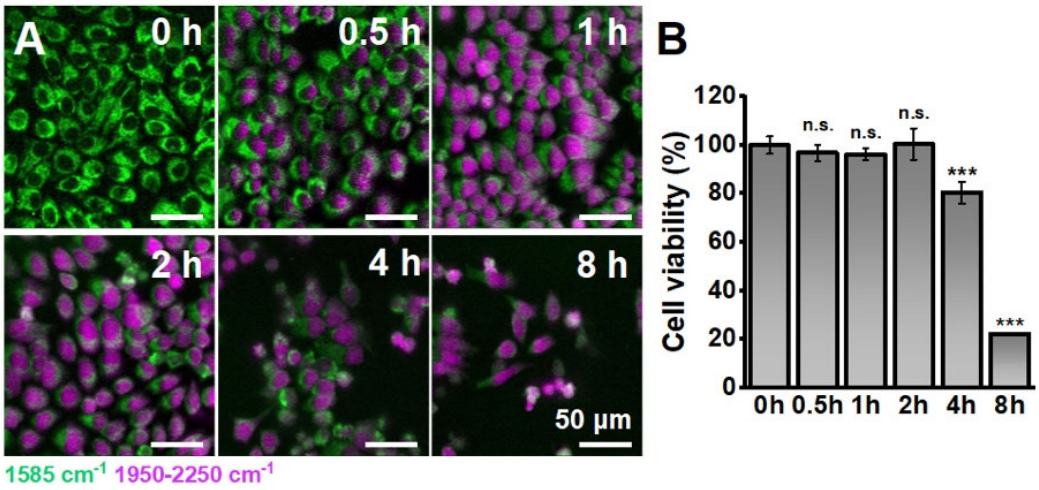

Figure 2. Simultaneous detection of the decrease in cyt *c* signal and drug uptake. HeLa cells were treated with 1 μM ActD and incubated for 0.5, 1, 2, 4 and 8 h. Cells without ActD treatment were used as controls. (A) The reconstructed Raman images at 1585 cm^{-1} and 1950-2250 cm^{-1} were merged to show localization of cyt *c* (green) and ActD (magenta), respectively. Scale bars, 50 μm. (B) Cell viability measured by MTT assay. The significant difference was compared with the most left box. ***: $P < 0.001$; n.s.: $P \geq 0.05$.

Evaluation of dose-dependent cytotoxicity by Raman microscopy

As a Raman-based assay can detect apoptotic events earlier than the MTT assay, we investigated the potential of using label-free Raman microscopy to unveil the dose-dependent induction of apoptosis by ActD. HeLa cells were treated with a gradient of ActD from 0 to 10 μM for 4 h. Reconstructed Raman images at 1585 cm^{-1}, 2850 cm^{-1}, and 2930 cm^{-1}, which can be assigned to cyt *c*, CH_2 symmetric stretching, and CH_3 symmetric stretching, are shown in Figure 3A. At the low dose (0.01 μM), the intensity of cyt *c* remained at a level similar to the vehicle control; at 0.1 μM, a clear decrease in cyt *c* signal was detected, and the same trend was maintained until the drug concentration reached 10 μM. The average Raman spectra of the cell cytoplasm (nuclear area was excluded) were extracted and compared in Figure 3B. The raw spectra of cell cytoplasm with residual background are shown in Figure S7. Since the Raman shift at 600, 750, 1127, and 1314 cm^{-1} were affected by ActD fluorescence at higher doses, we used 1585 cm^{-1} to investigate on cyt *c* dynamics. A dose-dependent decline of 1585 cm^{-1} was sensitively detected by label-free Raman microscopy.

Hyperspectral Raman imaging enables quantitative assessment at the single-cell level. To quantify the Raman intensity of cyt *c* at the single-cell level, segmentation of the whole cell body and nuclei was conducted using Cellpose, a deep learning-based segmentation program that was pretrained with a large dataset of cell images by the developer.[34] The detailed processing method is shown in the supporting information (Figure S6). The segmentation of cell cytoplasm (nuclei excluded) was created by subtracting nuclei from the whole cell body, and the average spectrum of cytoplasm was extracted. The number of cells utilized for the statistical analysis was 163, 191, 146, 125, and 98 cells for ActD concentrations of 0, 0.01, 0.1, 1, and 10 μM, respectively. To acquire average spectra of each cell, 410 ± 173 spectra in the cytosol area were averaged. For the comparison among different conditions, the intensity of target Raman shifts was normalized by 2930 cm^{-1}, which is assigned for CH_3 symmetric

stretching mode and empirically used as cell reference peak.[35] A significant decrease in cyt *c* intensity was detected at 0.1 μM with a large cell–cell difference (Figure 3C). The difference in ActD uptake could explain the large cell–cell difference, as already shown in Figure 1. However, the MTT assay showed a significant difference at 1 μM, with only a 20% decline compared to the control (Figure 3D), while Raman microscopy indicated a more drastic drop in the reduced cyt *c* signal.

It is well known that the redox state of cyt *c* is firmly associated with cell apoptosis.[36] Although early studies on cyt *c* demonstrated that changes in the redox state of cyt *c* were not necessary in cell apoptosis, later evidence indicated oxidized cyt *c* can induce caspase activation by binding with cytosolic adaptor protein Apaf1, whereas reduced cyt *c* cannot.[37] The oxidation of cyt *c* is likely due to endogenous oxidative machinery in mitochondria, as mitochondria isolated from apoptotic cells can oxidize cyt *c*, whereas mitochondria from healthy cells cannot.[38] However, it remains unclear whether oxidation begins before or after the release of cyt *c*. Our previous study showed that the redox state of cyt *c* was not significantly altered during the rapid release.[27] The present results indicated that the reduced cyt *c* decreased before its release when treated with a relatively high dose of ActD and incubated for relatively long periods of time (4 h) compared with our previous study (1 h). It should be noted that our previous study observed cyt *c*, which partially remained in the reduced form after 1 h of incubation with ActD and 6 h fresh medium without ActD (Figure S8).

Immunofluorescence staining of cyt *c* was performed to confirm the localization of cyt *c* after ActD treatment. Unreleased cyt *c* shows an intense mitochondria-like contrast, while the released cyt *c* is distributed throughout the cell body. We observed that a few cells started to release cyt *c* when treated with 0.1 μM ActD (Figure 3E, indicated by white arrow). Although the number of cells that initiated the release of cyt *c* increased from 0.1 μM to 10 μM, most cells did not start to release cyt *c* even at 10 μM. On the other hand, Raman

measurements indicated an overall decrease in reduced cyt *c* at higher doses (1 μM and 10 μM). This result suggested that the oxidation of cyt *c* occurred before its release into the cytosol. This is consistent with the fact that cyt *c* is converted into a peroxidase and oxidize cardiolipin in response to oxidative stress.[39] Oxidized cardiolipin recruits the pro-apoptotic protein tBID and Bax to outer mitochondrial membrane, which switch on the release of cyt *c* from the mitochondria to the cytosol. Oxidative stress, such as ROS generation, is associated with treatment of anticancer drug, including ActD,[40] which may be the trigger of oxidation of cyt c in the mitochondria. Thus, the decrease in reduced cyt *c* could be an apoptotic marker earlier than the release of cyt *c*. Raman microscopy sensitively detected the redox change of cyt *c* before its release into the cytosol, allowing for a more rapid and sensitive analysis of drug-induced cytotoxicity.

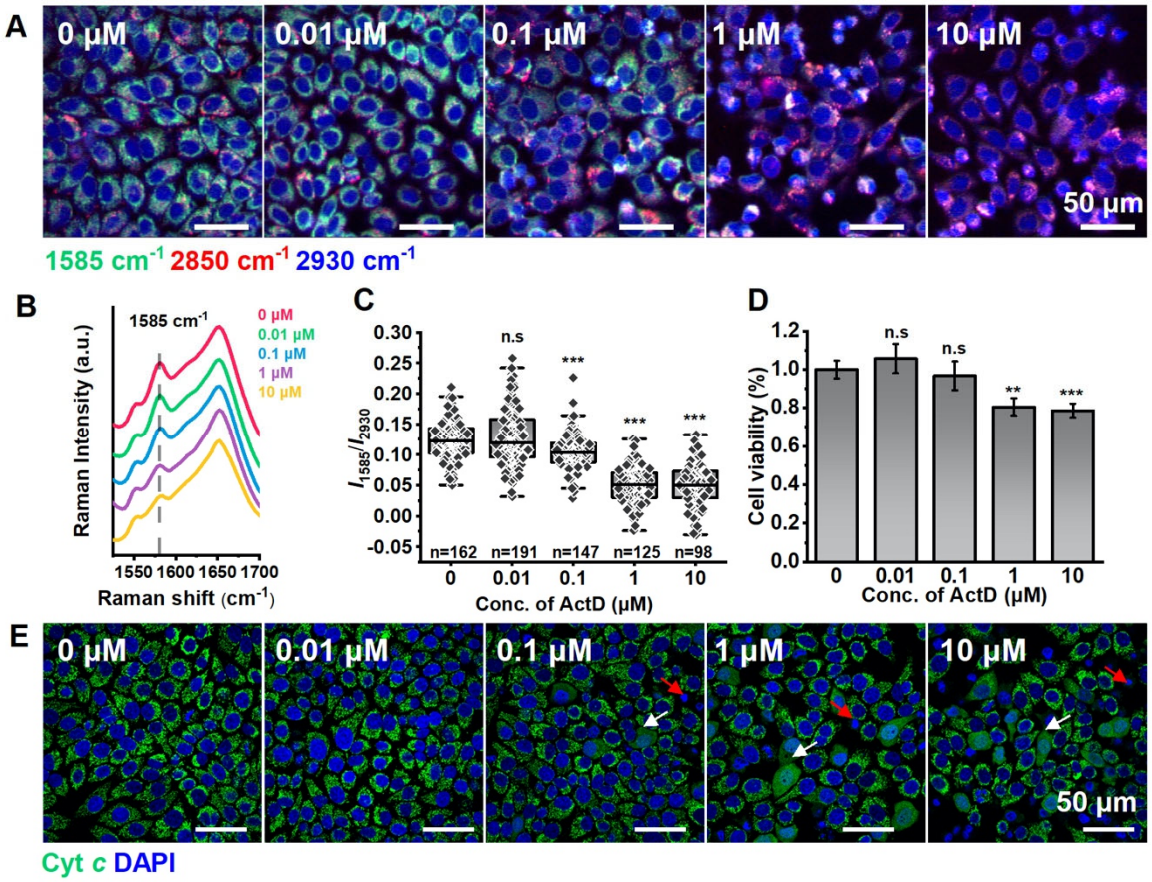

Figure 3. Raman measurement of dose-dependent cytotoxicity induced by ActD. HeLa cells were treated with ActD at different concentrations (0, 0.01, 0.1, 1, and 10 μM) for 4 h, and induced cytotoxicity was evaluated by Raman microscopy. (A) Reconstructed Raman images at 1585 cm^{-1}, 2850 cm^{-1}, 2930 cm^{-1}, which can be assigned to reduced cyt *c*, CH_2 symmetric stretching, and CH_3 symmetric stretching, respectively. A decrease in the cytochrome signal with increasing ActD concentration is indicated. Scale bars, 50 μm. (B) The average Raman spectrum of cytosol area. (C) The box plot of the normalized Raman intensity at 1585 cm^{-1} showed a dose-dependent decrease. Box plots illustrate the spread within cell populations (center line, median; box, quartiles; whiskers, 1.5× interquartile range). The significant difference was compared with the most left box. ***: $P < 0.001$; n.s.: $P \geq 0.05$. (D) Drug cytotoxicity measured by the MTT assay. The significant difference was compared with the most left box. ***: $P < 0.001$; **: $P < 0.01$; n.s.: $P \geq 0.05$. (E) Immunofluorescence image of cyt *c* (green) in HeLa cells treated with ActD at different concentrations. Cell nuclei were counterstained by DAPI (blue). Each white arrow indicates cells that initiated the release of cyt *c* with a diffuse distribution throughout the cell body. Each red arrow indicates condensed or broken nuclei. Scale bars, 50 μm.

Investigation on drug mechanism of action

One issue hindering elucidation of the mechanism of drug action is the lack of an efficient method to visualize the cellular response and drug concentration at the effector site. Therefore, we investigated the dose-dependent changes in drug uptake. We mapped the distribution of ActD by using autofluorescence signals (Figure 4A, upper lane). Drug uptake by cells showed an opposite trend to the decrease in cyt *c* signal (Figure 3A). After treatment with ActD for 4 h, a dose-dependent increase in the fluorescence signal of the cell nuclei was observed (Figure 4A, upper lane).

Furthermore, in the case of 10 μM treatment, we detected characteristic peaks of ActD at 1259 cm^{-1} and 1484 cm^{-1} assigned to the C-C=C and C-C=N stretching vibrations in the phenoxazone chromophore of ActD (Figure 4B).[24] The raw spectra with residual background were shown in Figure S9. A shift of 1266 cm^{-1} to 1259 cm^{-1} was detected compared with the Raman spectrum of 100 μM ActD in aqueous solution (Figure S1A). The same shift was confirmed when ActD was applied to the DNA solution (Figure S10), indicating that the DNA-bound ActD accumulated in the cell nuclei was detected. We did not observe the original 1266 cm^{-1} peak in the cell nuclei. Since the 1259 cm^{-1} peak was affected by the autofluorescence signal, we used 1484 cm^{-1} to describe the distribution of DNA-bound ActD (Figure 4A, lower lane). A clear contrast in the nucleus was observed, which is related to the mechanism of action of ActD. Notably, the characteristic peaks of ActD were much weaker in 10 μM ActD solution. (Figure S11). This result suggests that the concentration of ActD at its effector site is much higher than that in the culture medium, which would be useful to determine the effective dose of drug treatment.

We observed the blueshift and enhanced fluorescence once ActD entered the cells (Figure S1). This phenomenon has not been reported in live cell imaging. Due to the low quantum yield, this weak fluorescence might be difficult to detect using a conventional

fluorescence microscope, which is generally equipped with a low-power light source. Other Raman studies either using a longer wavelength (785 nm) or airdried cell samples did not report the observation of autofluorescence from ActD.[25, 41] We also confirmed that the shifted autofluorescence was not detected at 532 nm excitation after cell fixation (Figure S12). Furthermore, our observation showed that the fluorescence saturated faster in the cell nucleolus than in the nucleus when treated with 10 μM ActD for 30 min (Figure S13). Relatively long incubation led to shrinkage and damage to the cell nucleolus (Figure S14), and no nucleolar contrast of fluorescence was observed at 4 h (Figure 4A). This result suggested that ActD may first bind to rDNA or rRNA and that the nucleolus would be the first target of ActD treatment. Nucleolar RNA synthesis was reported more sensitive to ActD treatment.[42] Our result provides a direct support that ActD enriched firstly in cell nucleoli. This result suggested the importance of autofluorescence imaging in understanding drug uptake and subcellular localization.

However, the origin of this fluorescence is still unclear. We assume this fluorescence is due to the non-stacking binding of ActD to single-stranded DNA at the transcription or replication bubble. In aqueous solution, it was reported that 7-aminoactinomycin D (7-AAD), a fluorescent analog of ActD, can bind to single-stranded DNA with an increase in fluorescence intensity and a blueshift of the emission maximum.[43] The fluorescence properties of 7-AAD were found to be sensitive to different solvents, depending on solvent hydrogen bonding to the oxygen atom attached to the phenoxazone ring.[44] We compared the spectra of ActD in PBS, DNA, and denatured DNA. A blueshift to 620 nm and an increase in fluorescence were observed in the denatured DNA, whereas a decrease in fluorescence intensity was observed in natural dsDNA solution (Figure S15). Although a blueshift (to 620 nm) was observed in denatured solution, the emission maximum of ActD in the nuclei shifted more to approximately 567 nm (Figure S1B). However, no literature reported the blueshift to 567 nm. To our knowledge, this is the first report of autofluorescence signal induced by ActD treatment in

living cells. This result suggests one of possibilities that the fluorescence properties of ActD in living cells or the binding mode to DNA would be different under real physiological conditions.

Hyperspectral Raman imaging enables analysis at the subcellular level. To assess drug uptake at the effector site, we segmented the nuclei and extracted average spectra from individual nuclei (Figure S6). The spectra of each nucleus averaged 187 ± 62 pixels. The intensity of autofluorescence indicates the absorption of the drug, and the intensity of 1484 cm^{-1} indicates binding to DNA. Quantitative analysis (Figure 4C) confirmed the trend presented by hyperspectral Raman imaging (Figure 4A). To understand the correlation between the drug concentration and the subsequent effect on cyt *c* dynamics, we compared the intensity of cyt *c* (1585 cm^{-1}) with the intensity of autofluorescence and 1484 cm^{-1} in the same cells (Figure 4C and 4D). A clear difference was found between the low-dose group (0.01 μM and 0.1 μM) and the high-dose group (1 μM and 10 μM). At 0.1 μM, a fraction of cells was distributed toward high values of autofluorescent signals, indicating the initiation of drug uptake. At 0.1 μM ActD, there was a significant change in the cyt *c* intensity, indicating cytotoxicity triggered by drug uptake. The comparison of cyt *c* with 1484 cm^{-1} showed that the binding of ActD to DNA was still low at 0.1 μM, which explains the smaller attenuation of the cyt *c* signal compared to the higher dose.

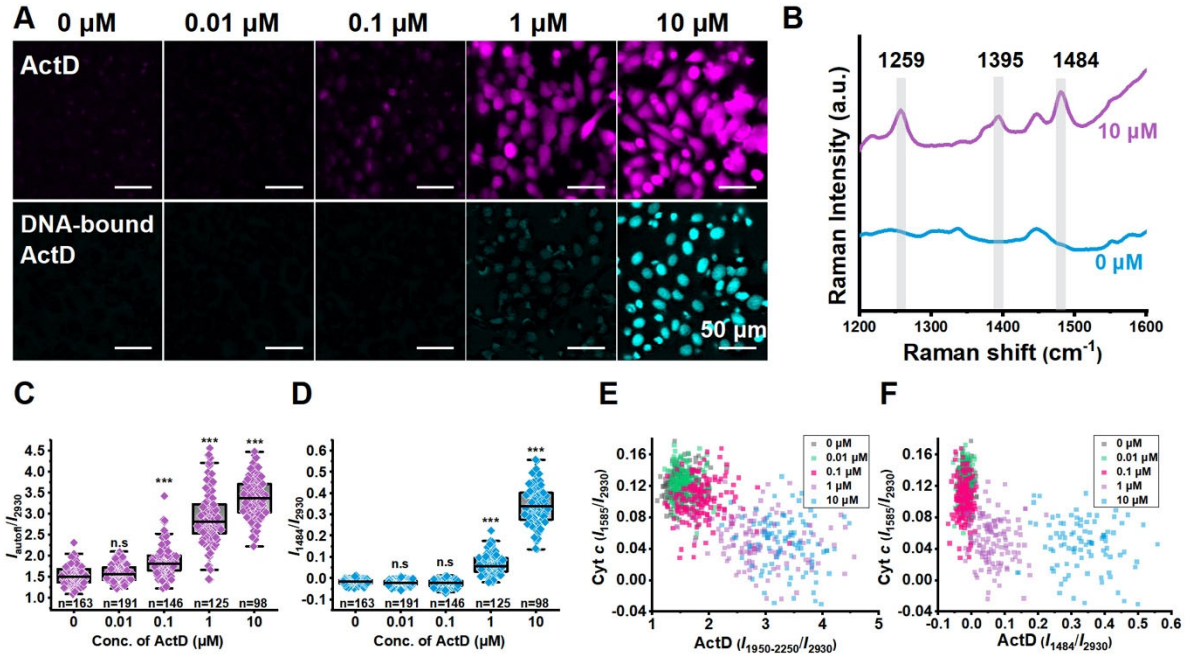

Figure 4. Investigation on cellular drug uptake at the single-cell level. (A) Reconstructed Raman images showing dose-dependent changes in drug uptake (upper lane, magenta) and DNA binding efficiency (lower lane, cyan). Scale bar: 50 μm. (B) Comparison of the average spectra of nuclei in cells treated with 0 μM and 10 μM ActD. The spectra were plotted with a vertical shift for comparison. The box plot of the normalized intensity of autofluorescence (C) and 1484 cm^{-1} (D) showed dose-dependent changes. Box plots illustrate the spread within cell populations (center line, median; box, quartiles; whiskers, 1.5× interquartile range). Comparison of cyt *c* intensity with the intensity of autofluorescence (E) and 1484 cm^{-1} (F) in the same cell. Statistical significance was evaluated by one-way ANOVA followed by post hoc Tukey–Kramer's range tests (compared with the left column/box). The significant difference was compared with the most left box. n.s.: $P \geq 0.05$; ***: $P < 0.001$.

CONCLUSION

In this research, we demonstrated the use of label-free Raman microscopy to evaluate cytotoxicity and visualize drug uptake simultaneously. Raman microscopy can sensitively detect time-dependent and dose-dependent changes in cyt *c* signaling induced by anticancer drugs. To assess the cytotoxicity of anticancer drugs, colorimetric assays, such as the MTT assay, have been utilized as effective first screening methods due to their high throughput and easy handling.[45] Subsequently, more sensitive apoptosis assays, such as caspase or cyt *c* release assays, have been used to understand the effects of drugs that trigger the apoptosis cascade. Our study provides a rapid and sensitive method for drug screening by targeting early apoptotic events. This method allows for us to screen the drug cytotoxicity and approach the mechanism at the same time, thereby reducing the cost and time of drug screening.

The spectroscopic feature of Raman microscopy enables the detection of molecular fingerprint of drug and the interaction at the target site. Here, we utilized the weak fluorescence of ActD to monitor drug uptake, whereas the appearance of characteristic peaks of ActD indicated the binding of ActD to DNA. The subsequent decrease in cyt *c* intensity was monitored in the same cell after drug uptake. We achieved simultaneous observation of cellular drug uptake and cytotoxicity by Raman microscopy, which would facilitate a precise understanding of pharmacological effects and predict potential drug toxicity in the future. The method described here can be adapted to investigating on the distribution of other drugs with weak autofluorescence, such as Doxorubicin. The uptake and the mechanism of action could be evaluated in living cells which would further facilitate drug development process.

METHODS

Cell culture

HeLa cells were seeded into 35-mm dishes (SF-S-D12; Fine Plus International) with quartz substrate (ø 12 mm) affixed to the bottom. Silicone rings with an inner diameter of 15 mm were placed on the dishes, and HeLa cells were plated at a density of 1.0×10^5 cells/ml. Quartz-bottom dishes were precoated with 0.01% collagen type 1 solution (IFP9660, Research Institute for the Functional Peptides) for 30 min at room temperature (RT). HeLa cells were cultured at 37°C in an atmosphere of 5% CO_2 in Eagle's minimum essential medium (MEM, M4655, Sigma–Aldrich) supplemented with 10% fetal bovine serum (10270106, Thermo Fisher) and antibiotics (100 U/ml penicillin G, 100 µg/ml streptomycin; 168-23191, Wako) for 48 h. To demonstrate the simultaneous observation of drug uptake and the effect on cyt *c*, cells were treated with 0.1 µM ActD (010-21263, Wako) for 4 h (Figure 1). Time-course investigation of ActD was performed at 1 µM and incubated for 0, 0.5, 1, 2, 4 and 8 h (Fig.Figure 2). The final concentrations of ActD at 0, 0.01, 0.1, 1, and 10 µM were applied to HeLa culture and incubated for 4 h (Figure 3 and 4).

Slit-scanning Raman microscopy

Raman measurements were performed using a homemade slit-scanning Raman microscope equipped with a 532 nm CW laser (Millennia eV, Spectra-Physics) with a power density of 3 mW/µm^2 (Figure 1) or 1 mW/µm^2 (Figure 2, 3, and 4) at the sample, as previously described.[26, 27] The laser light was shaped into a line using cylindrical lenses and focused on the sample using a water-immersion objective lens (CFI Apochromat Lambda S 40×, NA 1.25 or CFI75 Apochromat 25×, NA 1.1; Nikon) mounted on an inverted microscope (ECLIPSE Ti2-E, Nikon). The Raman scattered light was collected by the same objective lens. A 532-nm

longpass edge filter (LP03-532RU-25, Semrock) was used to block the excitation light and Rayleigh scattering light and allow Raman scattered light to pass into a spectrograph (MK-300; Bunkoukeiki). The light dispersed by the grating (600 l/mm) was then detected using a cooled CCD camera (PIXIS 400 B; Teledyne Princeton Instruments) with an exposure time of 5 s/line. 400 Raman spectra were collected on a single line. A single-axis galvanometer mirror was used to scan the images. For the high-resolution Raman image shown in Figure 1, 252 lines were scanned at a pitch of 0.333 μm, resulting in 100,800 (400 pixels × 252 lines) spectra in one image. In Figure 2, 3, and 4, 126 lines were scanned at a pitch of 1.6 μm and 50,400 (400 pixels × 126 lines) spectra were obtained in a single image with an acquisition time of less than 20 minutes.

Data processing

Raman hyperspectral images were processed as described previously.[27,28] Briefly, cosmic rays were removed by the median filter, singular value decomposition (SVD) was applied to reduce noise and loading vectors contributing to the image contrast were chosen. Following SVD processing, the peak area of individual Raman peaks was utilized to map the intensity distribution of the designated Raman shifts. Only for the autofluorescence signal, an average Raman intensity from 1950 cm^{-1} to 2250 cm^{-1} was applied to show the distribution.

Single-cell-based quantitative analysis was conducted after reconstruction of hyperspectral Raman images (Figure S6). The segmentation of cell bodies and nuclei was then performed with the Cellpose program. Cellpose is a deep learning-based segmentation program that was pretrained with a large dataset of cell images by the developer.[34] Raman images at 2930 cm^{-1} were utilized for the segmentation of the cell bodies, and contrast at 2930 cm^{-1} subtracted by the contrast at 1585 cm^{-1} was loaded for the segmentation of cell nuclei. The

segmentation results matched the loaded images shown in Figure S6. Cytoplasm contrast was created by subtracting the nuclei from the cell body. Then, the individual masks of cytoplasm and nuclei were applied to the Raman hyperspectral data. The Raman data were preprocessed with cosmic ray removal and moving averages to smooth the noisy data. The intensity of the target Raman shifts was calculated in terms of the peak area. The intensity of autofluorescence was calculated by averaging wavenumbers from 1950 cm^{-1} to 2250 cm^{-1}.

MTT assay

A commercially available MTT assay kit (11465007001, Roche) was utilized according to the manufacturer's protocol. HeLa cells were seeded and maintained in a 96-well glass-bottom plate. The seeding and culture conditions were the same as the Raman measurements. After treatment with ActD, 10 µl of the MTT labeling reagent was added to each well containing 100 µl of culture medium (final concentration 0.5 mg/ml). The microplates were incubated for 2 h at 37°C with 5% CO_2 to produce purple formazan crystals. Next, 100 µl of the solubilization solution was added to each well and incubated overnight to dissolve the formazan crystals. The absorbance of each well at 550 nm was measured using a microplate reader (Synergy HTX; BioTek). The absorbance at 650 nm was utilized as a background reference. The cell viability was calculated as a percent of the control.

Immunofluorescence staining

Immediately after ActD treatment, HeLa cells were fixed with 4% paraformaldehyde for 20 min at RT, permeabilized with 0.1% Triton X-100 (T8787, Sigma-Aldrich) in PBS for 10 min and blocked with 4% bovine serum albumin (A2153, Sigma–Aldrich) for 1 h at RT. A primary antibody working solution containing mouse monoclonal anti-cyt *c* (1:500, sc-13561, Santa

Cruz) was prepared in 1% bovine serum albumin solution, applied to the cell samples, and incubated overnight at 4°C. Then, the samples were washed three times with PBS and immersed in a secondary antibody solution containing Alexa Fluor 488 goat anti-mouse antibody (10 μg/ml, A11001, Invitrogen) for 1 h at RT. After washing with PBS three times, the cells were counterstained with 1 μM DAPI solution (D1306, Invitrogen) at RT. The cells were then washed twice with PBS, and the dishes were stored and protected from light at 4°C until image acquisition. Fluorescent images were captured using a confocal laser scanning microscope (A1; Nikon).

DNA experiment

Calf thymus DNA solution (10 mg/ml, 047-27511) was purchased from Wako. The working condition of the DNA solution was diluted to 1 mg/ml using PBS. DNA denaturation was performed by incubating DNA solution at 100°C for 10 min and cooling in an ice-water mixture. ActD was diluted to 50 μM in PBS, DNA solution, and denatured DNA solution. The Raman spectra of each condition were measured by using the same conditions as the cell experiment.

Statistical analysis

The quantitative data presented in this study were obtained from three independent cultures. Statistical analysis was first assessed with one-way analysis of variance (ANOVA), and individual differences were tested using post hoc Tukey–Kramer's range tests according to unequal sample sizes. All statistical calculations were performed using OriginPro 2021 (OriginLab Corporation, MA, USA). Statistical significance was set at $P < 0.05$. Symbols used are: ***: $P<0.001$; **: $P<0.01$; *: $P<0.05$; and n.s. (not significant)$P \geq 0.05$.

ASSOCIATED CONTENT

Supporting Information

The Supporting Information is available free of charge on the ACS Publication website.

Raman spectra of ActD in solution and in cell nuclei, Raman images of HeLa cells reconstructed at different wavenumbers that can be assigned to reduced cytochromes, optimization of power density, live/dead assay following Raman measurement, details of single-cell based quantification method, raw spectra of Hela cells treated with different concentration of ActD, Raman imaging of HeLa cells treated with ActD and prolonged incubation in fresh medium, Raw spectra of cell nuclei treated with or without ActD, Raman spectra of ActD in aqueous solution, DNA, denatured DNA, and cell nuclei; Raman images of fixed HeLa cells treated with ActD; Enrichment of ActD fluorescence in the nucleoli and effect on nucleoli structure (PDF).

AUTHOR INFORMATION

Corresponding Authors

Menglu Li – Department of Applied Physics, Osaka University, 2-1 Yamadaoka, Suita, Osaka 565-0871, Japan; AIST-Osaka University Advanced Photonics and Biosensing Open Innovation Laboratory, National Institute of Advanced Industrial Science and Technology (AIST), Suita, Osaka 565-0871, Japan; Email: menglu.li@ap.eng.osaka-u.ac.jp.

Katsumasa Fujita – Department of Applied Physics, Osaka University, 2-1 Yamadaoka, Suita, Osaka 565-0871, Japan; AIST-Osaka University Advanced Photonics and Biosensing Open Innovation Laboratory, National Institute of Advanced Industrial Science and Technology (AIST), Suita, Osaka 565-0871, Japan; Institute for Open and Transdisciplinary Research

Initiatives, Osaka University, 2-1 Yamadaoka, Suita, Osaka 565-0871, Japan; Email: fujita@ap.eng.osaka-u.ac.jp.

Author contributions: M.L. and K.F. conceived the concept; M.L., K.B., and K.F. designed the experiments; M.L. performed the experiments; M.L., H.L., K.B., and K.F. analyzed the data; Y.N. and S.F. provided tools for Raman measurement and analysis; M.L. and K.F. wrote the manuscript with input from H.L., K.B., Y.N., and S.F. All authors have read and agreed to the published version of the manuscript.

Notes: The authors declare no competing interests.

ACKNOWLEDGMENT

We thank Ms. K. Yamamoto for the help with the experiments. This research was supported by AIST-Osaka University Advanced Photonics and Biosensing Open Innovation Laboratory (PhotoBio-OIL). This study was partially supported by JST-CREST and JST COI-NEXT under Grant Numbers JPMJCR1925 and JPMJPF2009.

REFERENCES

(1) Chabner, B. A.; Roberts, T. G. Chemotherapy and the war on cancer. *Nat. Rev. Cancer* **2005**, *5*, 65-72.
(2) Evan, G. I.; Vousden, K. H. Proliferation, cell cycle and apoptosis in cancer. *Nature* **2001,** *411*, 342-348.
(3)Johnstone, R. W.; Ruefli, A. A.; Lowe, S. W. Apoptosis: A link between cancer genetics and chemotherapy. *Cell* **2002**, *108* (2), 153-164.
(4) Dollery, C. T. Intracellular drug concentrations. *Clin. Pharmacol. Ther.* **2013**, *93*, 263-266.
(5) Butler, H. J.; Ashton, L.; Bird, B.; Cinque, G.; Curtis, K.; Dorney, J.; Esmonde-White, K.; Fullwood, N. J.; Gardner, B.; Martin-Hirsch, P. L.; Walsh, M. J.; McAinsh, M. R.; Stone, N.; Martin, F. L. Using Raman spectroscopy to characterize biological materials. *Nat. Protoc.* **2016**, *11*, 664-87.
(6) Krafft, C.; Schmitt, M.; Schie, I.W.; Cialla-May, D.; Matthaus, C.; Bocklitz, T.; Popp. J.; Label-free molecular imaging of biological cells and tissues by linear and nonlinear Raman spectroscopic approaches. *Angew. Chem. Int. Ed. Engl.* **2017**, *56*, 4392-4430.
(7) Ember, K. J. I.; Hoeve, M. A.; McAughtrie, S. L.; Bergholt, M. S.; Dwyer, B.J.; Stevens, M. M.; Faulds, K.; Forbes, S.J.; Campbell, C. J. Raman spectroscopy and regenerative medicine: a review. *npj Regen. Med.* **2017**, *2*, 12.
(8) Yamakoshi, H.; Dodo, K.; Palonpon, A.; Ando, J.; Fujita, K.; Kawata, S.; Sodeoka, M. Alkyne-tag Raman imaging for visualization of mobile small molecules in live cells. *J. Am. Chem. Soc.* **2012**, *134*, 20681-20689.
(9) Yamakoshi, H.; Dodo, K.; Okada, M.; Ando, J.; Palonpon, A.; Fujita, K.; Kawata, S.; Sodeoka, M. Imaging of EdU, an alkyne-tagged cell proliferation probe, by Raman microscopy. *J. Am. Chem. Soc.* **2011,** *133*, 6102-6105.
(10) Chen, Z.; Paley, D. W.; Wei, L.; Weisman, A. L.; Friesner, R. A.; Nuckolls, C.; Min, W. Multicolor live-cell chemical imaging by isotopically edited alkyne vibrational palette. *J. Am. Chem. Soc.* **2014,** *136*, 8027-8033.
(11) Tipping, W. J.; Lee, M.; Serrels, A.; Brunton, V. G.; Hulme, A. N. Stimulated Raman scattering microscopy: an emerging tool for drug discovery. *Chem. Soc. Rev.* **2016,** *45*, 2075-2089.
(12) El-Mashtoly, S. F.; Petersen, D.;Yosef, H. K.; Mosig, A.; Reinacher-Schick, A.; Kotting, C.; Gerwert, K. Label-free imaging of drug distribution and metabolism in colon cancer cells by Raman microscopy. *Analyst* **2014**, *139*, 1155-1161.
(13) Aljakouch, K.; Lechtonen, T.; Yosef, H. K.; Hammoud, M. K.; Alsaidi, W.; Kötting, C.; Mügge, C.; Kourist, R.; El-Mashtoly, S. F.; Gerwert, K. Raman microspectroscopic evidence for the metabolism of a tyrosine kinase inhibitor, Neratinib, in cancer cells. *Angew. Chem. Int. Ed.* **2018**, *57*, 7250-7254.
(14) Farhane, Z.; Bonnier, F.; Byrne, H. J. Monitoring doxorubicin cellular uptake and trafficking using *in vitro* Raman microspectroscopy: short and long time exposure effects on lung cancer cell lines. *Anal. Bioanal. Chem.* **2017**, *409*, 1333-1346.
(15) Salehi, H.; Derely, L.; Vegh, A. G.; Durand, J. C.; Gergely, C.; Larroque, C.; Fauroux, M. A.; Cuisinier, F. J. G. Label-free detection of anticancer drug paclitaxel in living cells by confocal Raman microscopy. *Appl. Phys. Lett.* **2013**, *102*, 113701.
(16) Feofanov, A. V.; Grichine, A. I.; Shitova, L. A.; Karmakova, T. A.; Yakubovskaya, R. I.; Egret-Charlier, M.; Vigny, P. Confocal raman microspectroscopy and imaging study of theraphthal in living cancer cells. *Biophys. J.* **2000**, *78*, 499-512.
(17) Majzner, K.; Wojcik, T.; Szafraniec, E.; Lukawska, M.; Oszczapowicz, I.; Chlopicki, S.; Baranska, M. Nuclear accumulation of anthracyclines in the endothelium studied by bimodal imaging: fluorescence and Raman microscopy. *Analyst* **2015,** *140*, 2302-2310.

(18) Hollstein, U. Actinomycin. Chemistry and mechanism of action. *Chem. Rev.* **1974,** *74*, 625-652.
(19) Krugh, T. R. Association of Actinomycin D and deoxyribodinucleotides as a model for binding of the drug to DNA. *Proc. Natl. Acad. Sci. U. S. A.* **1972,** *69*, 1911-1914.
(20) Sobell, H. M. Actinomycin and DNA transcription. *Proc. Natl. Acad. Sci. U. S. A.* **1985,** *82*, 5328-5331.
(21) Kersten, W. Interaction of actinomycin C with constituents of nucleic acids. *Biochim. Biophys. Acta Bioenerg.* **1961**, *47*, 610-611.
(22) Chinsky, L.; Turpin, P. Y. Fluorescence of actinomycin D and its DNA complex. *Biochim. Biophys. Acta.* **1977**, *475*, 54-63.
(23) Chinsky, L.; Turpin, P. Y.; Duquesne, M.; Brahms, J. Resonance Raman study of actinomycin D interaction with DNA and its models. *Biochem. Biophys. Res. Commun.* **1975,** *65*, 1440-1446.
(24) Smulevich, G.; Angeloni, L.; Marzocchi, M. P. Raman excitation profiles of actinomycin-DNA complex. *Spectrochim. Acta A* **1982,** *38*, 219-221.
(25) Farhane, Z.; Bonnier, F.; Byrne, H. J. An *in vitro* study of the interaction of the chemotherapeutic drug Actinomycin D with lung cancer cell lines using Raman micro-spectroscopy. *J. Biophotonics* **2018**, *11*, e201700112.
(26) Palonpon, A. F.; Ando, J.; Yamakoshi, H.; Dodo, K.; Sodeoka, M.; Kawata, S.; Fujita, K. Raman and SERS microscopy for molecular imaging of live cells. *Nat. Protoc.* **2013**, *8*, 677-692.
(27) Okada, M.; Smith, N. I.; Palonpon, A. F.; Endo, H.; Kawata, S.; Sodeoka, M.; Fujita, K. Label-free Raman observation of cytochrome *c* dynamics during apoptosis. *Proc. Natl. Acad. Sci. U. S. A.* **2012**, *109*, 28-32.
(28) Hamada, K.; Fujita, K.; Smith, N. I.; Kobayashi, M.; Inouye, Y.; Kawata, S. Raman microscopy for dynamic molecular imaging of living cells. *J. Biomed. Opt.* **2008**, *13* (4), 044027.
(29) Kakita, M.; Kaliaperumal, V.; Hamaguchi, H. O. Resonance Raman quantification of the redox state of cytochromes *b* and *c in-vivo* and *in-vitro*. *J. Biophotonics* **2012**, *5*, 20-24.
(30) Mosmann, T. Rapid colorimetric assay for cellular growth and survival: application to proliferation and cytotoxicity assays. *J. Immunol. Methods* **1983**, *65*, 55-63.
(31) Morimoto, T.; Chiu, L. D.; Kanda, H.; Kawagoe, H.; Ozawa, T.; Nakamura, M.; Nishida, K.; Fujita, K.; Fujikado, T. Using redox-sensitive mitochondrial cytochrome Raman bands for label-free detection of mitochondrial dysfunction. *Analyst* **2019**, *144*, 2531-2540.
(32) Loveland, B. E.; Johns, T. G.; Mackay, I. R.; Vaillant, F.; Wang, Z. X.; Hertzog, P. J. Validation of the MTT dye assay for enumeration of cells in proliferative and antiproliferative assays. *Biochem. Int.* **1992**, *27*, 501-510.
(33) Stepanenko, A. A.; Dmitrenko, V. V. Pitfalls of the MTT assay: Direct and off-target effects of inhibitors can result in over/underestimation of cell viability. *Gene* **2015**, *574*, 193-203.
(34) Stringer, C.; Wang, T.; Michaelos, M.; Pachitariu, M. Cellpose: a generalist algorithm for cellular segmentation. *Nat. Methods* **2020**, *18*, 100-106.
(35) Fournier, F.; Gardner, E. M.; Kedra, D. A.; Donaldson, P. M.; Guo, R.; Butcher, S. A.; Gould, I. R.; Willison, K. R.; Klug, D. R. Protein identification and quantification by two-dimensional infrared spectroscopy: Implications for an all-optical proteomic platform. *Proc. Natl. Acad. Sci. U. S. A.* **2008**, *105*, 15352-15357.
(36) Brown, G. C.; Borutaite, V. Regulation of apoptosis by the redox state of cytochrome *c*. *Biochim. Biophys. Acta.* **2008**, *1777*, 877-881.

(37) Hampton, M. B.; Zhivotovsky, B.; Slater, A. F.; Burgess, D. H.; Orrenius, S. Importance of the redox state of cytochrome *c* during caspase activation in cytosolic extracts. *Biochem. J.* **1998**, *329*, 95-99.
(38) Borutaite, V.; Brown, G. C. Mitochondrial regulation of caspase activation by cytochrome oxidase and tetramethylphenylenediamine via cytosolic cytochrome *c* redox state. *J. Biol. Chem.* **2007**, *282*, 31124-31130.
(39) Kagan, V. E.; Tyurin, V.A.; Jiang, J.; Tyurina, Y.Y.; Ritov, V.B.; Amoscato, A.A.; Osipov, A.N.; Belikova, N.A.; Kapralov, A.A.; Kini, V.; Vlasova, I.I.; Zhao, Q.; Zou, M.; Di, P.; Svistunenko, D.A.; Kurnikov, I.V.; Borisenko, G.G. Cytochrome *c* acts as a cardiolipin oxygenase required for release of proapoptotic factors. *Nat. Chem. Biol.* **2005**, *1*, 223-232.
(40) Ricci, J.E.; Gottlieb, R.A.; Green, D.R. Caspase-mediated loss of mitochondrial function and generation of reactive oxygen species during apoptosis. *J. Cell Biol.* **2003**, *160,* 65-75.
(41) Farhane, Z.; Nawaz, H.; Bonnier, F.; Byrne, H. J. *In vitro* label-free screening of chemotherapeutic drugs using Raman microspectroscopy: Towards a new paradigm of spectralomics. *J. Biophotonics* **2018**, *11*, e201700258.
(42) Bensaude, O. Inhibiting eukaryotic transcription: Which compound to choose? How to evaluate its activity? *Transcription* **2011**, *2*, 103-108.
(43) Wadkins, R. M.; Jovin, T. M. Actinomycin D and 7-aminoactinomycin D binding to single-stranded DNA. *Biochemistry* **1991**, *30*, 9469-9478.
(44) Vekshin, N.; Savintsev, I.; Kovalev, A.; Yelemessov, R.; Wadkins, R. M. Solvatochromism of the excitation and emission spectra of 7-Aminoactinomycin D: implications for drug recognition of DNA secondary structures. *J. Phys. Chem.* **2001**, *105*, 8461-8467.
(45) Riss, T. L.; Moravec, R. A.; Niles, A. L.; Duellman, S.; Benink, H. A.; Worzella, T. J.; Minor, L. Cell Viability Assays. 2013 May 1 [Updated 2016 Jul 1; Accesed 2022 June 15]. In: Markossian S, Grossman A, Brimacombe K, et al., editors. Assay Guidance Manual [Internet]. Bethesda (MD): Eli Lilly & Company and the National Center for Advancing Translational Sciences; 2004. Available from:
https://www.ncbi.nlm.nih.gov/books/NBK144065/?report=classic

Table of contents graphic